The Electronics of Thin Film Organic Photovoltaics

Seamus A. Curran[1], James Dewald[2], Amrita Haldar[2], Nigel Alley[2], Shawn Liao[2]

[1]CNTG, Physics Department, Science and Research Building 1, University of Houston, Houston, TX 77204, USA

[2]Physics Department, Science and Research Building 1, University of Houston, Houston, TX 77204, USA

Abstract

In this chapter, the aim is to investigate how the donor/acceptor interface of OPV devices affects the performance. In the second section of this chapter this effect is studied by using a bi-layer (p-n junction morphology) instead of a blended one, for the photoactive, the aim is to understand excitonic effects. From this it's possible to fabricate base junction devices using a bi-layers (p-n junction morphology) instead of a blended one, for the photoactive layer. In the fabrication of the p-n junction OPV device, dynamic spin coating is used as a deposition technique. After the first layer of P3HT is spin-coated onto the substrate, PCBM is then deposited using dynamic spin coating. By varying the spin-coating parameters, a device structure of ITO/PEDOT:PSS/P3HT/PCBM/Al with a range of P3HT/PCBM interface morphologies, from low level inter-digitated structure to direct flat contact, is demonstrated. Device PCEs are correlated to the film thickness and interface morphology of the active layer. In the fabrication of the p-n junction OPV device, dynamic spin coating is used as a deposition technique. After the first layer of P3HT is spin-coated onto the substrate, PCBM is then deposited using dynamic spin coating. By varying the spin-coating parameters, a device structure of ITO/PEDOT:PSS/P3HT/PCBM/Al with a range of P3HT/PCBM interface morphologies, from low level inter-digitated structure to direct flat contact, is demonstrated.

Introduction

In the last few decades great efforts in OPVs have been made[1-3], leading to promising successes with power conversion efficiencies (PCEs) reaching as high as 8%, most of which are based upon the bulk hetero-junction OPV architecture[4-6]. This complex blending structure has proved to be critical in solving one of the challenges for OPVs — the short exciton diffusion length (~ 10 nm)[7]. The abundance of significant donor/acceptor interfaces have given rise to a high exciton dissociation efficiency, one of the crucial processes Figure 1 required to efficiently convert light into usable current[8].

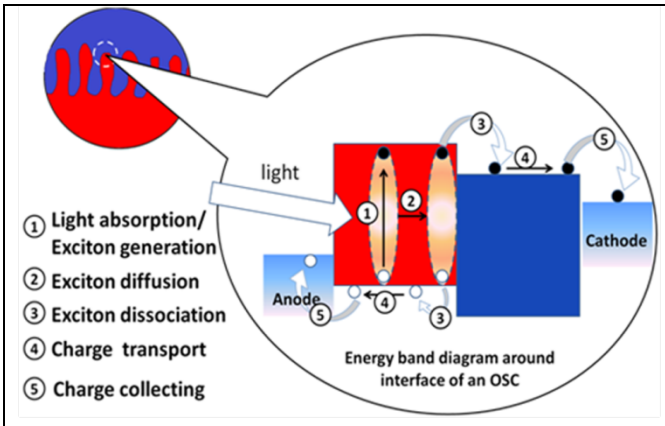

Figure 0. Schematic drawing of the five sequential steps converting light into photocurrent.

As research on bulk heterojunction layers has progressed to a significant degree of maturity from its beginning when Sariciftci et al. first demonstrated its effectiveness[9], additional charge collection improvements become more elusive. Whether marginal changes in morphology through annealing techniques, new photoactive polymers, new device architecture or examining in more detail the interfacial materials[10-14], progress is step-wise and slow. More recently, there has been an increased interest in combining the large phase separation regions in bulk heterojunctions with domains possessing high order percolating paths Figure 2 which has the potential to achieve high charge transport efficiency. In effect, by looking at the interface between

the p and n species in a bulk heterojunction, the question arises whether there is a more effective manner in combining both — as in a p-n junction layer structure.

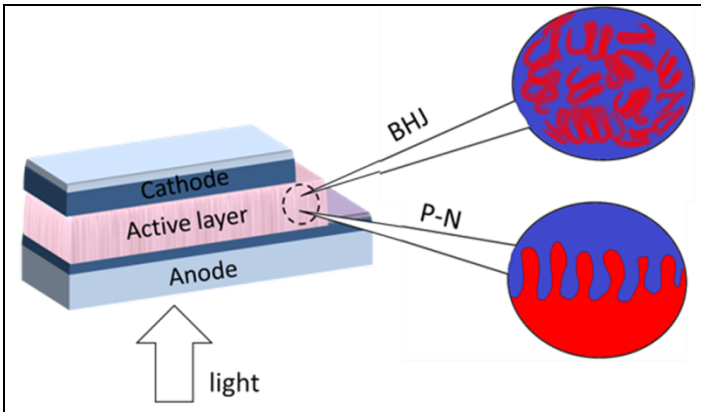

Figure 1. Schematic drawings of bulkheterojunction and the p-n junction architecture with a cross finger interface morphology.

Numerous efforts have been made to realize this effective structural combination. Forrest *et al.* believed that by introducing vertical phase separation to obtain a highly interconnected and entangled interpenetrating network, the series resistance in the organic bulk heterojunction can be reduced, thus impeding carrier extraction. They applied organic vapor phase deposition (OVPD) in fabrication of the photo-generation layer of copper phthalocyanine (CuPc) and C_{60}. The two materials were arranged in a way that when the second layer (C_{60}) was deposited onto the first layer (CuPc), before reaching full coverage, another layer of CuPc would be applied onto C_{60}, so the third layer was also in contact with the first layer. By continuously repeating this process, 3D interpenetrating nanocrystalline networks of CuPc and C_{60} could be formed. Their device yields a PCE of ~ 4.5%[15].

Besides the structure of the interpenetrating multilayer, a bilayer interdigitated morphology as shown in the schematic representation in Figure 1 is frequently mentioned as an ideal structure to enhance exciton dissociation and charge extraction simultaneously by optimizing the interface in the p-n junction layer into an ordered bulk heterojunction[16-18]. The high aspect ratio of this interdigitated structure can potentially increase device performance by

enhancing the delicate balance between phase separation and crystallinity. At present, nanoimprint lithography[17] and glancing angle deposition[19] are typically employed in achieving this structure. Using nanoimprint lithography, He *et al.* fabricated a comb wedge structured cell. A Si mode with a featured pattern size of between 25~200 nm was used to pattern the first film on a suitable substrate, then the patterned first film was used as a mold to imprint the second film, resulting in a double imprinted OPV device. Their device yields a PCE of ~2.3%, improving upon their bulkheterojunction control group with a PCE of 1.9%[17]

Brett et al., grew CuPc nanocolumns on ITO maintaining diameters of 40 - 50 nm using glancing angle deposition, precise length and width control of the nanorods were explored, aiming to apply this technique as another substitution in realizing the ideal morphology[19]. However, the high cost of vacuum evaporation as well as that of glancing angle deposition limits their application when attempting to scale up to industrial production. Also, the delicate imprinting scale in nanoimprint technique results in a series of crucial problems which are still waiting to be solved. In this case, solution processing will still be the more preferred way to industrial production for its cheap and easy processing. The major issue to be addressed in this method is the difficulty in depositing two uniform polymer layers sequentially for the p-n junction photoactive device.

Theory

Band theory was introduced when R. de L. Kronig and W. G. Penney developed a one dimensional model for the electron interaction in a periodic potential in 1931[2]. In the model an infinite one dimensional array of finite potential wells with the dimension of the lattice constant were used to simulate the electron environment.

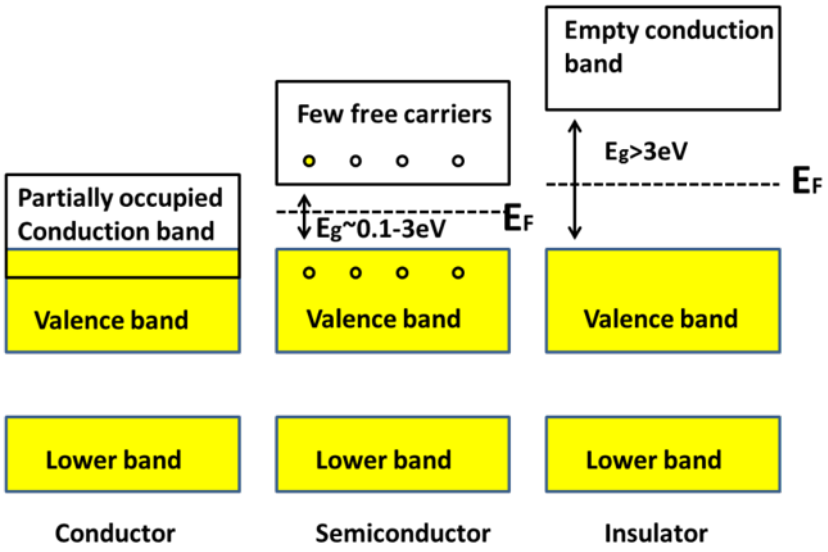

Figure 1-1. Electronic band structures for conductors, semiconductors and Inuslators, diagram redrawn and adapted from [1]

Forbidden energy levels around the Brillouin zone boundary were observed in their theory. In band theory the individual energy levels become irrelevant and only the band diagram for the entire crystal will be discussed. The entire band structure will be summarized by two discrete levels as mentioned before, the conduction band and the valance band. The Schrödinger equation for the electrons in the crystal may be written as[3]:

$$\left\{-\frac{\hbar^2}{2m}\nabla^2 + V(r)\right\}\Psi_k = \varepsilon(k)\Psi_k$$

In which $V(r)$ is the periodic potential energy seen by an electron from the lattice; $\varepsilon(k)$ is the energy of the electron; m is the electron mass. Due to the periodicity of the potential energy, the solution Ψ_k to this equation can be written in the form of Bloch waves:

$$\Psi_k(r) = e^{ikr}u_k(r)$$

Where $u_k(r)$ is the Bloch lattice function and $\Psi_k(r)$ is the Bloch wavefunction which will have periodicity throughout the crystal. Plenty of models have been applied in studying the band structures in the solid materials. As for metals, the electronic structures are typically calculated

with the nearly free electron model which assumes that electrons can move almost freely through the crystal lattice; while in the study of polymer semiconductors or conductors, the tight binding approximation is frequently applied. The most frequently used band theories for semiconductors are the orthogonalized plane wave method[4] and the pseudo-potential method[5].

The Parabolic Band Approximation

At times when we discuss the electric phenomena in semiconductor, only the charges located near the maximum of the valence band and the minimum of the conduction band are of interest, this is due to the fact that after vibration relaxation that is where the free moving charge carriers will be found. Near the minimum of the conduction band and the maximum of the valance band we can use parabolic functions obtained from a Taylor expansion to approximate the energy band as [6]:

$$E_{e,h}(\vec{k}) = E_{e,h}(0) \pm \frac{\hbar^2 \vec{k}^2}{2m^*}$$

In which $E_{e,h}(0)$ is the minimum energy in conduction band and maximum energy in valence band, respectively; m^* is the effective mass for electron which takes in account the electron mass as well as the effect of internal force between the electron and other particles in the semiconductor material. It is defined as:

$$m^* = \hbar^2 [\frac{d^2 \varepsilon(k)}{dk^2}]^{-1}$$

The effective mass of the charge carriers will depend on the curvature of the energy band.

Direct and Indirect Band Gap Semiconductors

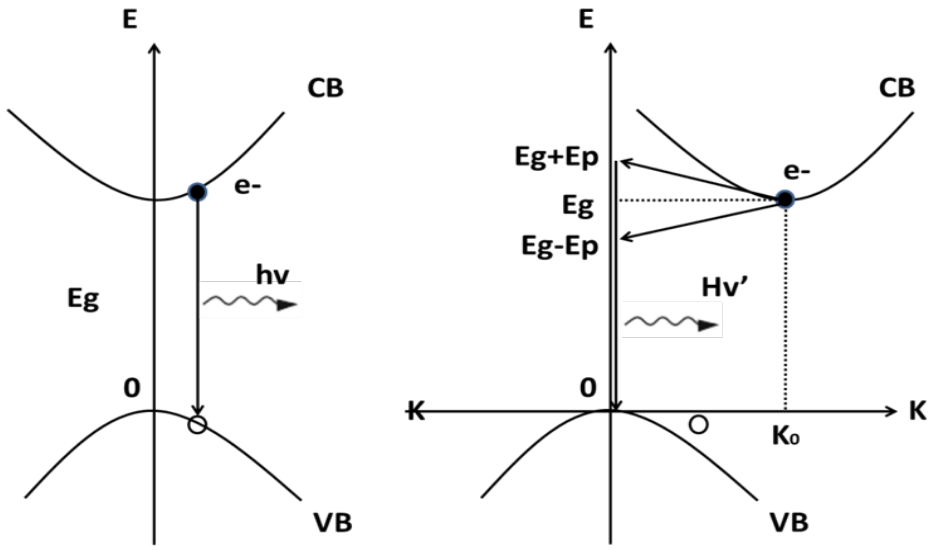

Figure 1-2. Electron transition in direct (left) and indirect (right) semiconductors, diagram redrawn from [7]

The energy band diagram is plotted as a function of crystal momentum (k-vector) as shown in Table 1-2. If the minimum energy of the conduction band is achieved with the same k-vector of the maximum energy in the valence band, the semiconductor is said to have a direct band gap; otherwise it has an indirect band gap. For the excitation of the electrons from valence band to conduction band, both conservation of energy and crystal momentum needs to be achieved, thus it will be much easier for it occur in a direct band gap semiconductor as the electron momentum doesn't change. While for an indirect band gap semiconductor, not only does a photon with energy larger or equal to the band gap have to be absorbed by the material, but also a phonon in order to keep balance with the electron momentum shift. The involvement of the phonon makes the radiative process much less likely to occur within a particular time interval. The absorbance of a direct band gap semiconductor can be hundreds of times higher than that of one possessing an indirect band gap, this is the reason why a thick silicon film has to be fabricated in the solar device as a compromise of its low light absorbance. The Table 1-1 shows the band gap information of some inorganic semiconductors.

	Material	Direct/Indirect bandgap	Band Gap energy at 300 K (eV)
Elements	C (diamond)	Indirect	5.47
	Ge	Indirect	0.66
	Si	Indirect	1.12
	Sn (grey)	Direct	0.08
Groups	GaAs	Direct	1.42
Compounds III-V	InAs	Direct	0.36
	InSb	Direct	0.17
	GaP	Indirect	2.26
	GaN	Direct	3.36
	InN	Direct	0.70
Groups	α-SiC	Indirect	2.99
Compounds IV-IV			
Groups	ZnO	Direct	3.35
Compounds II-VI	CdSe	Direct	1.7
	ZnS	Direct	3.68

Table 1-1. Band gap value for some inorganic semiconductor materials. Table rebuilt from [8]

One of the most important and basic ideas in semiconductor device physics is that of a p- n junction. It is well known that a semiconducting material can be doped with impurities which are either capable of donating electrons or accepting electrons. A semiconductor that is doped with donor impurities is an n-type semiconductor. This means that the impurity energy level lies close to the bottom of the conduction band, and the donor impurity is capable of donating electrons to the conduction band. A semiconductor that has acceptor impurities is referred to as a p-type semiconductor. In this case, the impurity energy level lies close to the top of the valence band, and is capable of accepting electrons from the semiconductor's valence band (leaving behind holes in the valence band). For any standard semiconductor at room temperature, kT << EG. In this case, the Fermi level must lie between the impurity level and its corresponding band. This means that for an n-type semiconductor, the Fermi level lies

very close to the bottom of the conduction band, while for a p-type semiconductor, the Fermi level lies very close to the top of the valence band. When these two types of materials are brought into contact, a p- n junction is formed. At first, electrons and holes move through this junction in such a way as to establish an equilibrium state (in the absence of an applied external voltage) which brings the Fermi levels of the two types to a constant value throughout the sample. This equilibrium is established as follows. The n-type side has a surplus of electrons, and so electrons diffuse into the p-type side. Similarly, the p-type side has a surplus of holes, Intrinsic and Extrinsic Semiconductors

When an electron is excited from the valence band to the conduction band, a hole is left in the valence band. When no impurities are doped into the semiconductor and the electron density equals the hole density, it is called an intrinsic semiconductor. We will identify the electron and hole densities as n and p, respectively. When semiconductors are doped with materials that are added to provide free carriers, it is called an extrinsic semiconductor. The dopant giving additional electrons to the conduction band are called donors, donor energy level is below the conduction band within an interval ~kT. Thus the electrons in the donor energy level may jump to the conduction band due to thermal activation, leaving an ionized positive charge in the donor energy level. Similarly, an acceptor energy level will stay around the thermal energy ~kT higher than that of valence band, thus the electrons in the valance band can jump to the impurity energy level. The semiconductor with ionized donor will be called n-type and the one with acceptor impurity will be called p-type.

Density of States

The number of occupied conduction energy states due to thermal excitation is given as[9]:

$$n = \int_{E_c}^{E_{top}} g(E)F(E)dE$$

Where E_c is the energy at the bottom of the conduction band and E_{top} is the energy at the highest level of the conduction band; $F(E)$ is the possibility that the energy E is occupied by an electron and will be Fermi distribution; g(E) is the density of states defined as the number of states with energy less than E. By calculating the number of states within the volume with radius k we write:

$$N = \frac{2 \times \frac{4}{3}\pi k^3}{(\frac{2\pi}{l})^3} = \frac{k^3 l^3}{3\pi^2}$$

$$\frac{dN}{dE} = \frac{dN}{dk}\frac{dk}{dE} = (\frac{l}{\pi})^3 \pi k^2 \frac{dk}{dE}$$

Using the parabolic approximation, we can write the energy of the electrons as:

$$E(k) = \frac{\hbar^2 k^2}{2m^*}$$

So density of states g(E) per unit volume is:

$$g(E) = \frac{1}{l^3}\frac{dN}{dE} = \frac{\sqrt{2}}{\pi^2 h^3} m^{*\frac{3}{2}}\sqrt{E}$$

Carrier Densities and Fermi Energy in Equilibrium[10]

If the Fermi energy level is more than 3kT away from either side of the band edge, we call the semiconductor non-degenerate. In this case, the Fermi distribution can be simplified to a Maxwell-Boltzmann distribution. After integrating on both sides of Equation we can get:

$$n = N_C e^{\frac{E_i - E_C}{kT}} = p = N_V e^{\frac{E_V - E_i}{kT}}$$

Where N_C and N_V are the effective density of states for the conduction and the valence band, respectively:

$$N_C = 2(\frac{2\pi m_e^* kT}{h^2})^{\frac{3}{2}}$$

$$N_V = 2(\frac{2\pi m_p^* kT}{h^2})^{\frac{3}{2}}$$

The effective mass for the electrons and holes are:

$$m_e^* = \hbar^2[\frac{d^2 E_c(k)}{dk^2}]^{-1}$$

$$m_h^* = -\hbar^2[\frac{d^2 E_V(k)}{dk^2}]^{-1}$$

And the Fermi level in intrinsic semiconductor E_i equals to:

$$E_i = \frac{E_C + E_V}{2} + \frac{1}{2} kT ln \frac{N_V}{N_C}$$

It mostly lies in the middle between the conduction band and the valence. We can also have the mass action law:

$$np = n_i^2 = N_C N_V e^{\frac{-E_g}{kT}}$$

In which n_i is the intrinsic carrier density and is equal to the density of electrons which are thermally excited into the CB of a pure semiconductor; E_g is the band gap energy.

Quasi Fermi Energy

When disturbance is introduced to the semiconductor such as the exposure to light with photon energy larger than semiconductor band gap, the electrical injection of electrons through an applied electric bias or the doping to the material, the density of the charge carriers in the semiconductor will be higher than the equilibrium values, in which case we cannot apply the Fermi Dirac equilibrium distribution function in solving the carrier densities any longer and the relationship of $n = p = n_i$ will no longer stand. However, we could assume that the electrons and holes can each achieves a quasi-thermal equilibrium, after which all the electrons in the conduction band share a common electron quasi Fermi level E_{F_n} and the holes in the valence band shares a hole quasi Fermi level E_{F_p}, with analogy to Equations , we can write[9]:

$$n = N_C e^{\frac{E_{F_n} - E_C}{kT}}$$

$$p = N_V e^{\frac{E_V - E_{F_p}}{kT}}$$

Looking at the charge density in terms of n_i instead of density of states:

$$n = n_i e^{\frac{E_{F_n} - E_i}{kT}}$$

$$p = n_i e^{\frac{E_i - E_{F_p}}{kT}}$$

Where E_i and n_i are the Fermi level and the equilibrium charge density in intrinsic semiconductor, respectively. Rearrange these two equations we can write out the Fermi level in quasi thermal equilibrium or in extrinsic semiconductor[10] as:

$$E_{F_n} = E_i + kTln\frac{n}{n_i}$$

$$E_F = E_i - kTln\frac{p}{n_i}$$

Where n and p will be the total majority electron and hole densities in the semiconductor, respectively. From the two equations it is clear that the Fermi energy will shift upward to the conduction band in donor doped semiconductor (n-type) and downward to the valence band in acceptor doped semiconductor (p-type), as shown in Figure 1-3.

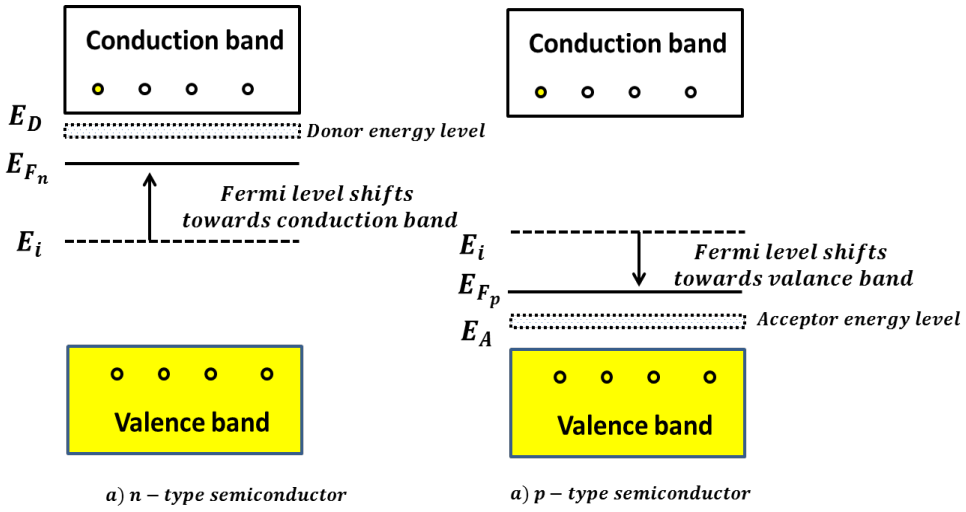

Figure 1-3. Energy band diagrams in extrinsic semiconductors, diagrams redrawn from [11]

The difference in quasi Fermi levels is the difference in chemical potentials (the same as Fermi level) $\Delta\mu$. The mass action law is now written as:

$$np = n_i^2 e^{\Delta\mu/kT}$$

Where:

$$\Delta\mu = E_{F_n} - E_{F_p}$$

Doping in Conjugated Polymer

Most linear conjugated polymers such as polyacetylene or polyparaphenylene with a π system along the polymer chain are often semiconductors or insulators, however, it was discovered that an increase in conductivity can be achieved by applying redox chemistry to these intrinsically insulating polymers. This chemical treatment is also called "doping" analogous to the doping in inorganic semiconductors. However, instead of applying additives into the inorganic semiconductors, the "doping" in organic polymers is the process of oxidation or reduction of a polymer system. The use of an oxidizing agent to the polymer corresponds to p-type doing; while the use of a reducing agent corresponds to n-type doping.

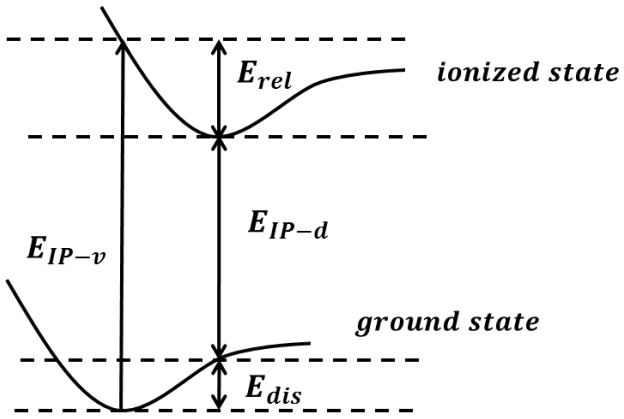

Figure 1-9. Illustration of the energies involved in a molecular ionization process. Diagram redrawn from[21]

For organic molecules, it is usually the case that the molecule or electron geometry in equilibrium ionized state is different than that of the ground state. As shown in Figure 1-9, the lowest energy in the ionized state of the molecule is shifted away to a different k-vector from where ground state achieved its minimum energy. A vertical Franck-Condon like ionization is processed with an excitation energy of E_{IP-v}, after that a geometry relaxation happens with a

release of energy E_{rel}. However, this process can also be achieved by a molecule which first distorts to the equilibrium ionized geometry when it is still in the ground state, and then process the excitation directly to the equilibrium ionized state with an excitation energy of E_{IP-d}. The distortion energy required by the molecule is E_{dis}. In the one-electron energy level of the molecule, the distortion will correspond to an upward shift $\Delta\varepsilon$ of the HOMO level and a downward shift of the LUMO level.

Polarons

As mentioned above, after the addition/reduction of one electron from an organic polymer, it is energetically favorable to localize the charge on the polymer chain and have a local distortion around the charge. This radical ion associated with the lattice distortion is called a polaron, and the formation of the polaron will introduce an energy level $\Delta\varepsilon$ below/above the LUMO/HOMO level called the polaron energy level, as shown in Figure 1-10 (The figure shows a positive polaron formed by the extraction of an electron from the semiconductor). The relaxation energy E_{rel} is also called the polaron binding energy, and is measured to be in the order of 0.05 eV in polyamide (PA), 0.03 eV in poly(p-phenylene) (PPP) and 0.12 eV in Polypyrrole (PPy)[21]. When the doping continues and more polarons are formed in the polymer, polaron band will be formed and thus the conductivity goes up. To introduce an electron polaron, an electron will be taken from the donor or from photoexcitation, and is added to the upper polaron level; To introduce a hole polaron, an electron from the lower polaron level will go to the acceptor or a hole will created by photoexcitation[22]. The evolution of the band structure from that in a pristine polymer to polaron bands merged with the valence and conduction band is shown in Figure 1-10.

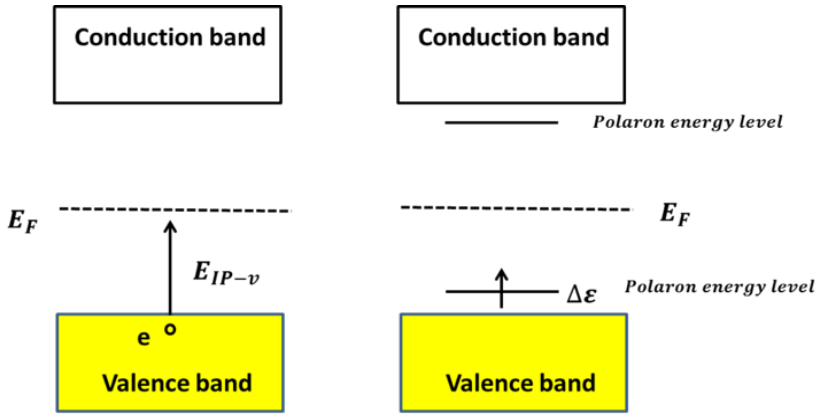

Figure 1-10. Band structure of a polymer chain without (left) and with (right) a p+ polaron level. Diagram redrawn from[21].

Bipolarons

Bipolarons are formed at heavy doping levels. A bipolaron is the radical ion and the lattice distortion in the polymer chain when a second electron is added or removed from the existing polaron. The formation of a bipolaron implies a strong lattice distortion as the interaction of the bipolaron with the lattice needs to be larger than the coulomb repulsion between the two charges to make the structure stable. Thus in the electronic band structure, the energy level of a bipolaron will be further away from the band edges than the one in polaron, as shown in Figure 1-11. The bipolaron binding energy E_{rel}^{bip} will be larger than that of two polarons for about 0.45 eV as measured in PPy and 0.34 eV in PPP[21]. Hence one bipolaron is thermodynamically more stable than two polarons in the polymer. In case of positive (negative) charges, the polaron levels are empty (fully occupied) and the bipolaron is a spinless quasiparticle. Therefore there is no optical transition between the lower and the upper bipolaron levels.

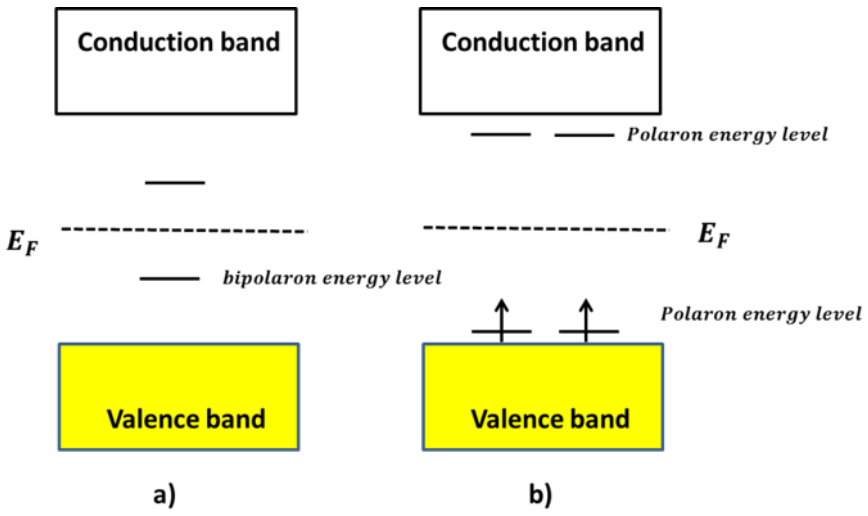

Figure 1-11. Band structure of a polymer chain with a) a p+ bipolaron and b) two p+ polarons. Diagram redrawn from[21].

Solitons

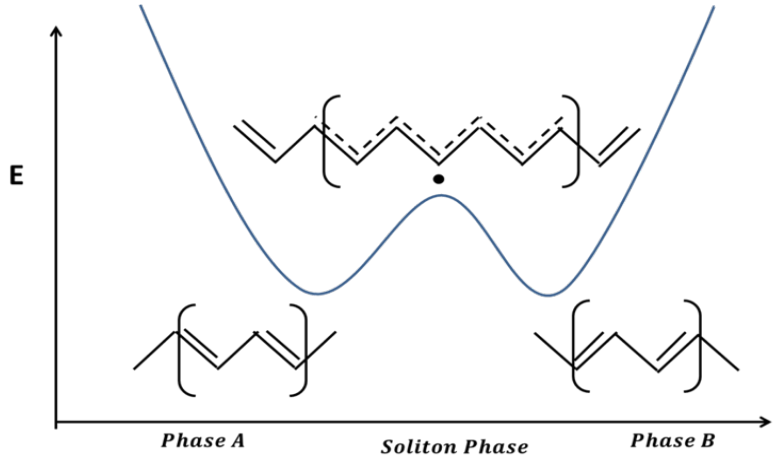

Figure 1-12. The energy curve for an infinite trans-polyacetylene chain with three difference configuration structures. Diagram redrawn from[17].

If a polymer has two possible geometric structures corresponding to the same total energy, it then possesses a degenerate ground state. A typical polymer in this case is Polyacetylene. As the result of the energy degeneracy, a bipolaron formed in this type of polymer can be easily separated as there is no increase in distortion energy for this process. The two different structures with the same energy level will be distributed on different segments that are separated by the charge; in this case, the charge associated with a boundary is called a soliton. The presence of the soliton

will lead to the appearance of a localized electronic level at mid-gap between conduction and valence band, which will be half occupied for a neutral soliton formed with odd number of conjugated carbons in the system and empty/full occupied for a positively/negatively charged soliton[23]. A charge delocalization is also found around the soliton.

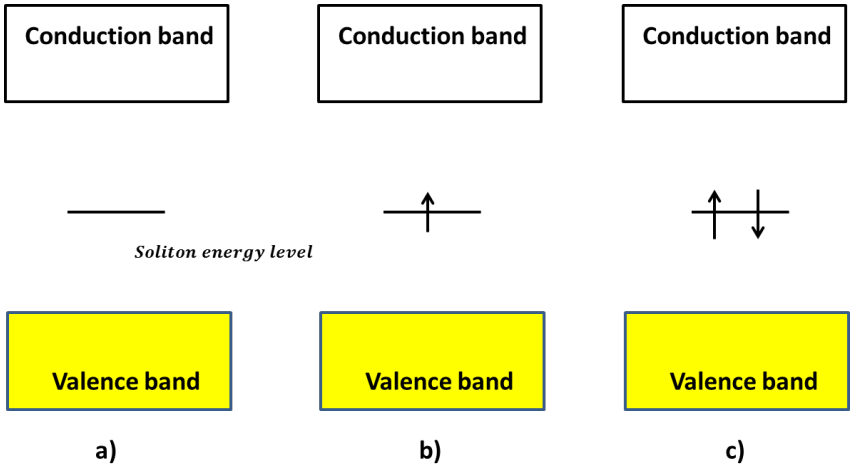

Figure 1-13. Band structure for a trans-polyacetylene chain containing a) a positively charged b)neutral c) negatively charged soliton. Diagrams redrawn from[17].

Excitons

Wannier Excitons

In semiconductors with high dielectric constant, excitons with radius of the order of ten times the lattice constant can be found, this type of exciton is called a Wannier or a Wannier-Mott exciton. Wannier excitons are mostly found in inorganic systems, where the electron-hole interaction energy is small (a few meV typically). Considering the coulomb potential between the electron and hole pair as:

$$U(r) = -\frac{e^2}{4\pi\varepsilon_0\varepsilon r}$$

Where r is the distance between the electron and hole; ε is the dielectric constant of the material, typically $\varepsilon \geq 10$ for inorganic semiconductors[24]. Taking coulombic interaction as the only force between the electron-hole pair, we can apply the Bohr model of the hydrogen atom to the free Wannier exciton and solve for the binding energy level of the electron-hole pair. Before applying the hydrogen electron model number of adjustments are required; unlike the real hydrogen atomic system, which is composed of a very heavy nucleus and a negligible electron, the electron-hole system is formed by two quasi-particles with comparable masses. Additionally, the Coulomb force between the electron and hole in a Wannier exciton will be largely screened by the dielectric constant. In this case, an effective mass is used to replace the proton mass in the hydrogen atom:

$$m_r = \frac{{m_e}^* {m_h}^*}{{m_e}^* + {m_h}^*}$$

and after including a dielectric constant ε in the energy level expression,[25] the binding energy of a Wannier exciton can be written as

$$E_{X(n)} = \frac{\frac{m_r}{m_0}}{\varepsilon^2}\frac{1}{n^2}Ry(H) = \frac{E_X}{n^2}$$

In which m_0 is the free electron mass and Ry(H) = 13.6 eV refers to the ground state of the hydrogen atom, also known as Rydberg binding energy; ${m_e}^*({m_h}^*)$ is the electron (hole) effective mass; E_X is the binding energy at ground level and n is the energy level. Comparing the two binding energies E_X and $Ry(H)$, it is cleare that the Wannier exciton binding energy is around three orders of magnitude smaller than the hydrogen binding energy.

The free Wannier exciton can move throughout the lattice. Taking the assumption that it has kinetic energy:

$$E_{kin} = \frac{\hbar^2 K^2}{2(m_e + m_h)}$$

the total energy of a Wannier exciton in the lattice as [25] may be expressed as

$$E_{(n)}(K) = E_g - E_{X(n)} + E_{kin} = E_g - \frac{(\frac{m_r}{m_0})}{\mathcal{E}^2}\frac{Ry(H)}{n^2} + \frac{\hbar^2 K^2}{2(m_e + m_h)}$$

where K is the exciton wave vector; E_g is energy band gap of the lattice between conduction band and the ground state of the ideal pure crystal. The exciton energy level is depicted in Figure 1-14.

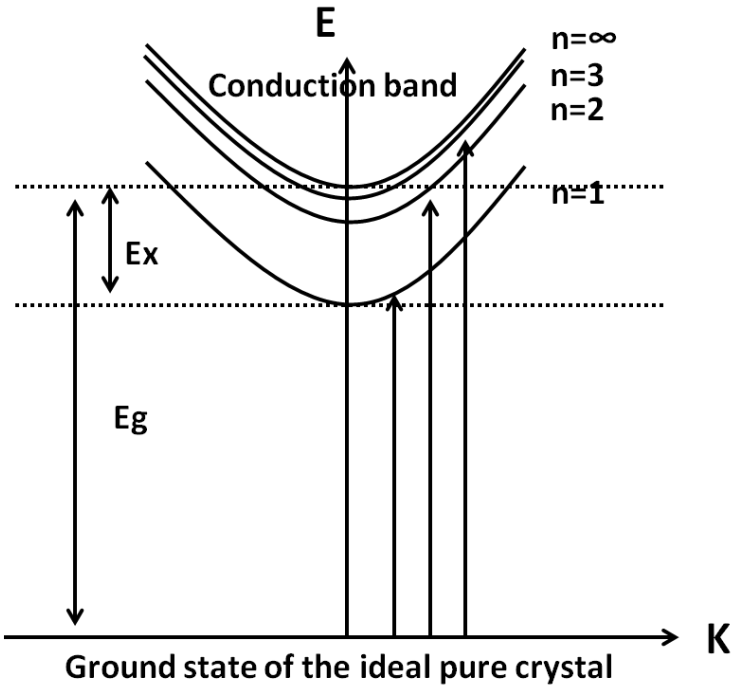

Figure 1-14. Excitation energy of an e-h pair in a Wannier excition as a function of translational wave vector K, optical absorption transitions are also marked. Diagram redrawn from[25].

Frenkel Excitons

In 1931 the concept of excitation waves in crystals was introduced and the term "exiton" was invented by a Russian theorist Yakov Frenkel to explain the photoemission lines observed in the spectra of organic molecular crystals[26]. Later the Frenkel exciton was used to represent excitons with strong coulomb interactions between the excited electron and the hole in the semiconducting material with a small dielectric constant. The binding energy of the exciton is approximately 100~300 meV and its radius is small whilst the electron-hole pair resides on the same molecular site. Frenkel excitons are typically found in organic molecular crystals composed of benzene rings such as anthracene and naphthacene.

If we consider the system as a linear crystal lattice with N identical molecules, each with one spinless electron, the periodic Eigen-functions of electrons can be written in a Bloch state [27]:

$$\Psi_K = N^{-\frac{1}{2}} \sum_m \quad [exp\ exp\ (iKR_m)\ ]\phi_m$$

Here the expression of Eigen-functions Ψ_K satisfies the normalization condition; ϕ_m is the Slater determinant of the electronic configuration when only the electron in the mth molecule at R_m is excited. K is the wave vector. We take the interactions between molecules as perturbation and apply the tight-binding model for a one electron Bloch state, the Eigen-values corresponding to the N split states can be written as [28]:

$$E(K) = E_n + \delta\omega_n + 2\beta\ cos\ cos\ (kd)$$

In which E_n is the energy of the exited atomic level, $\delta\omega_n = \delta\epsilon - \delta\omega_{n0}$ where $\delta\epsilon$ is the change in the cohesive energy per molecule and $\delta\omega_{n0}$ is the shift of the center of the exciton band on the nth energy level. β is the interaction between neighboring atoms, d is the nearest neighbor

separation. A scheme illustrating this energy state splitting and the energy level shifts parameters is shown in Figure 1-15.

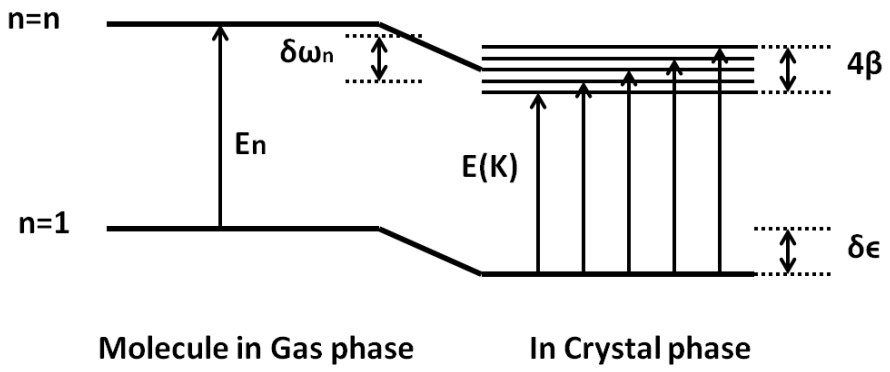

The I-V characteristic plots for five pixel devices in a comb electrode layout are shown in Figure 8.1. A linear rise in photo-generated current is observed as the number of devices connected in parallel increases from one to five. The very closely matched open circuit voltages observed indicates that the spin-coated layers are homogenous and contain few defects such as pinholes.

The I-V characteristic plots for five pixel devices in a comb electrode layout from the aforementioned publication are shown in Figure 8.1. A linear rise in photo-generated current is observed as the number of devices connected in parallel increases from one to five. The very closely matched open circuit voltages observed indicates that the spin-coated layers are homogenous and contain few defects such as pinholes.

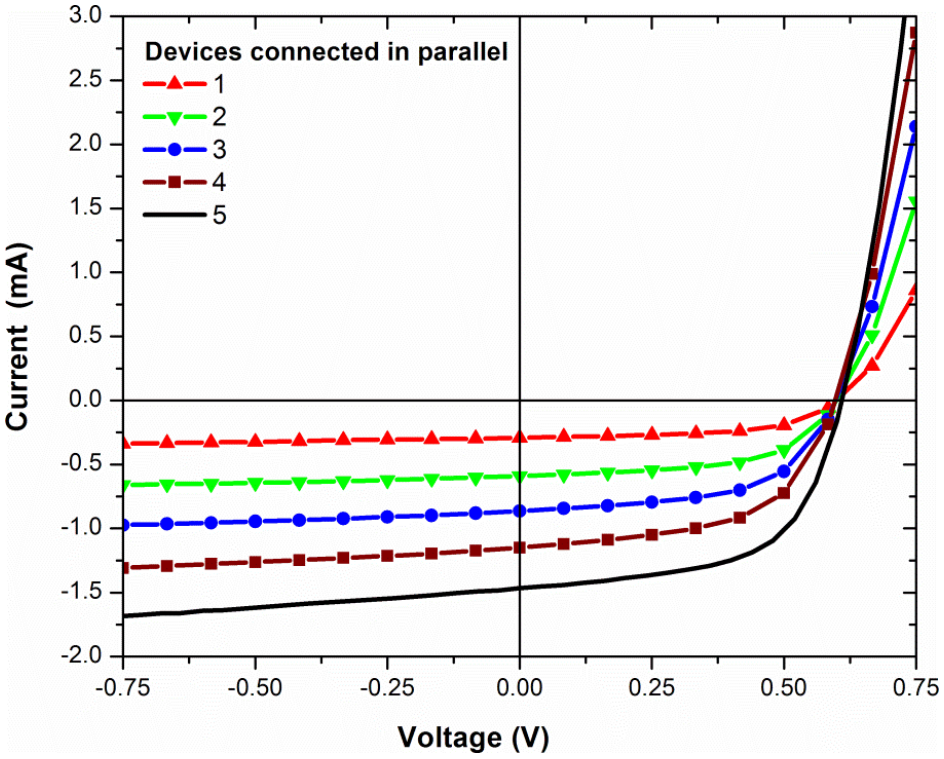

Figure.8.1: I-V characteristics of a 5 pixel comb electrode layout device [8]

Figure 8.2 is a comparison of the I-V trace of the five devices connected in parallel to that of the summation of the measured currents of the five individual pixels. It is clear that the two I-V characteristics shown are very similar suggesting that the comb electrode layout allows the efficient interconnection of pixel devices with very little loss of energy.

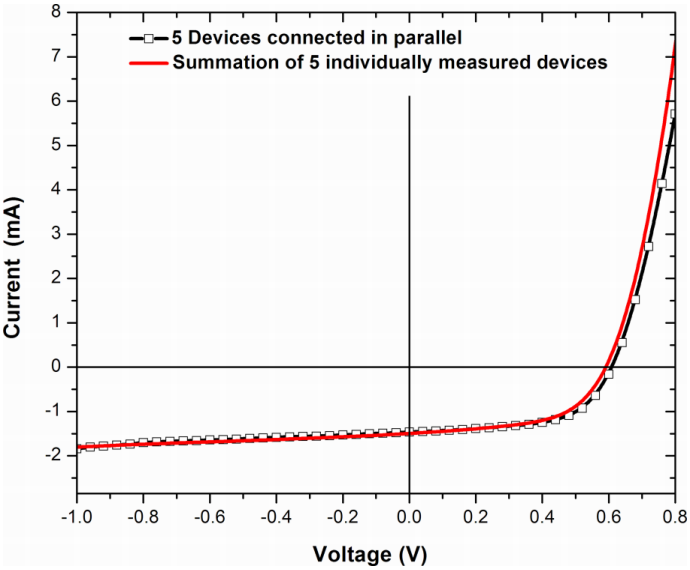

Figure 8.2: I-V characteristics of five devices connected in parallel to the summation of the same devices when individually measured.

Conclusion

Much discussion has been about exciton generation, carrier transport. In 1961 Shockley and Queisser published an article entitled "Detailed Balance Limit of Efficiency of p-n Junction Solar Cells" where they detailed a theoretically justified upper limit on the efficiency of a standard p-n junction Si solar cell [2]. Their calculations took into account an ideal case where the only recombination mechanism was radiative and another case where it was a fraction of the total recombination with the remainder being non-radiative. The illumination form the sun was approximated by a blackbody at 6000 K and the solar cell was assumed to behave as one at 300 K. The active-layer is assumed to be thick enough to absorb all incident solar radiation with energies higher than the band gap.

It was found that under perfect conditions where all absorbed light is converted to charge carriers and allowing for no losses due to contact or series resistance, a solar cell utilizing a material with a bandgap of 1.09 eV would have a maximum possible or 'ultimate efficiency' of 44 %. When considering some inherent limiting properties of Si, the detailed balance limit yields a reduced efficiency ~26 % and a maximum of ~30 % for a material having a bandgap of ~1.2

eV. Shockley and Quiesser state that the true physical limit is probably slightly less as a result of a certain rate of unavoidable non-radiative transitions and it should lie between a previously calculated empirical limit of 21.7% and that of the detailed balance limit of 26%. In OPV's currently, accounting for the lack of precisely tailored materials having ideal conductivity and optical transparency properties the actual maximum efficiency is far lower. Taking into account the external quantum efficiency a more realistic value for the Jsc is of the order of 12 – 16 $mAcm^{-2}$ [3] and efficiencies of champion cells ~ 10% or modules with efficiencies ~ 2-4%.

The design accommodates the requirement that the active layer is relatively thin of the order of 30-100 nm in order to achieve optimal exciton dissociation and charge collection given the percolating nature of charge transport within bulk-heterojunction OPVs. The dichotomy associated with this scenario is evident in terms of light lost due to the inherent optical transparency of such a thin layer. The thickness of the active layer in the OPV stack architecture needs to be reduced to allow an improved exciton dissociation efficiency due to the active layer being a smaller multiple of the exciton diffusion length of 5-20 nm [6]. Currently, these is a need to compromise absorption over exciton dissociation and carrier mobility or vice versa in a new device architecture.

References

[1] Green, M. A., Emery, K., Hishikawa, Y., & Warta, W. (**2011**). Progress in Photovoltaics: Research and Applications, *19*, 84-92.

[2] Shockley, W., & Queisser, H. J. (**1961**). *Journal of Applied Physics*, *32*, 510.

[3] Dennler, G., Scharber, M. C., & Brabec, C. J. (**2009**). *Advanced Materials*, *21*, 1323.

[4] Liao, K.-S., Yambem, S. D., Haldar, A., Alley, N. J., & Curran, S. A. (**2010**). *Energies*, *3*, 1212-1250.

[5] Curran, S. A., Talla, J., Dias, S., & Dewald, J. (**2008**). *Journal of Applied Physics*, *104*, 064305.

[6] Hoppe, H., & Sariciftci, N. S. (**2006**). *Journal of Materials Chemistry*, *16*, 45-61.

[7] Dias, S. (**2010**). *Novel Architectural Designs for Highly Efficient Organic Photovoltaic Devices*. University of Houston.

[8] Liao, K.-S., Dias, S., Alley, N. J., Yambem, S. D., Haldar, A., & Curran, S. A. (**2010**). *Thin Solid Films*, 10-13.

[9] Dennler, G., Forberich, K., Scharber, M. C., Brabec, C. J., Tomiš, I., Hingerl, K., Fromherz, T., & Tomiš, I. (**2007**). *Journal of Applied Physics*, *102*, 054516.

[10] Filmetrics. (n.d.). *Refractive Index Database: PET/Estar-Melinex-Mylar*. Retrieved from http://www.filmetrics.com/refractive-index-database/PET/Estar-Melinex-Mylar.

[11] Hecht, E. (**1990**). *Optics* (2nd ed.). Addison-Wesley.

[12] Pedrotti, F. L., Pedrotti, L. M., & Pedrotti, L. S. (**2007**). *Introduction to Optics*. Pearson Prentice Hall.

[13] Han, J. (**2005**). Proceedings of the 18th Annual ACM Symposium on User Interface Software and Technology, 115-118.

[14] Zhu, S. (**1986**). *American Journal of Physics*, *54*, 601.

[15] Alley, N. J., Dias, S., Liao, K.-S., & Curran, S. A. (**2012**). *Journal of Applied Physics*, *111*, 064914.